PROTEINS: Structure, Function, and Genetics 4:165–172 (1988)

Structural Analysis of the 2.8 Å Model of Xylose Isomerase From *Actinoplanes missouriensis*

Felix Rey[1], John Jenkins[1], Joel Janin[1], Ignace Lasters[2], Philippe Alard[2], Michel Claessens[2], Gaston Matthyssens[3], and Shoshana Wodak[2,4]

[1]*Laboratoire de Biologie Physicochimique, Universite Paris Sud, 91405 Orsay, Cedex France,* [2]*Plant Genetic Systems, CP160 P2 Universite Libre de Bruxelles, Avenue P. Heger 1050 Brussels, Belgium,* [3]*Plant Genetic Systems, Plateaustraat 22, 9000 Gent, Belgium,* [4]*Unite de Conformation de Macromolecules Biologiques, CP160 P2 Universite Libre de Bruxelles, Avenue P. Heger 1050 Brussels, Belgium*

ABSTRACT **The structure of Xylose isomerase (X.I.) from *Actinoplanes missouriensis* has been solved to 2.8 Angstroms resolution. Phases were determined from a single Eu^{3+} derivative and from the noncrystallographic 222 symmetry of the tetrameric molecule. An atomic model was built and subjected to restrained crystallographic refinement. The resulting model is shown to be closely similar to the recently reported X.I.'s structures from three other bacterial sources. Each monomer is found to be composed of an eight-stranded α/β "T.I.M." barrel forming an N-terminal domain of 328 residues followed by a large loop of 66 residues embracing an adjacent subunit. Analysis of intersubunit packing shows that the X.I. tetramer is an assembly of two tight dimers. The β barrel fits a simple hyperboloid model as other T.I.M. barrels do. The active site, identified as the binding site for the inhibitor xylitol, is located at the carboxyl end of the beta strands in the barrel next to a pair of binding sites for Eu^{3+} ions, which are assumed to be sites for the divalent ions involved in catalysis. Active sites in the tetramer are oriented towards the interface between dimers. It is suggested that subunit interfaces might stabilize the active site region and this might explain the oligomeric nature of other α/β barrel enzymes.**

Key words: α/β barrels, crystal structure, glucose isomerase, xylose isomerase

INTRODUCTION

Xylose isomerase (X.I.) catalyzes the isomerization of xylose to xylulose. Divalent metal ions (Mg^{2+} or Mn^{2+}) are required for the X.I. activity.[1] X.I. also isomerizes glucose to fructose,[2] albeit with a lower specific activity. Hence, the widespread use of X.I. in industrial processes involving the production of HFCS (high-fructose-containing syrups). In addition to the inherent interest of unraveling this protein structure, the study of the X.I. molecule can be put in a broader context. Indeed, the enzyme contains a domain which is folded as an eight-stranded α/β barrel. First described[3] in the case of Triose phosphate isomerase (T.I.M.) it has since been observed in many other enzymes. As the sequences of these enzymes are not homologous, the possibility of convergent versus divergent evolution for these proteins has been raised.[4] To arrive at a proper understanding of this type of protein architecture, it is mandatory to study as many α/β proteins as possible. The structural comparison of these proteins may ultimately provide clues explaining the success of this protein fold.

In this paper we describe the 2.8 Å x-ray structure of X.I. from *Actinoplanes missouriensis* with emphasis on the characteristics of the β barrel geometry and the mode of organization of the subunits within this oligomeric protein.

MATERIALS AND METHODS

Diffraction Data Collection

Xylose isomerase from *Actinoplanes missouriensis* was obtained from Gist Brocades, Delft, Holland. Crystals were grown in 1.2 M ammonium sulfate, pH 6.8 at 18°C by the hanging drop method. They form hexagonal bipyramids over 1 mm in size. Precession photographs show the space group to be $P3_121$ or $P3_221$ with parameters a = b = 143 Å, c = 2231.5 Å. The true space group was found to be $P3_221$. The asymmetric unit is a tetramer of molecular weight of 173,200, solvent occupying 68% of the crystal volume. The diffraction pattern extends beyond 2 Å.

Crystals were transferred into 1.7 M ammonium sulfate and mounted in glass capillaries. Diffracted intensities were collected by film techniques using the LURE-DCI synchrotron beam and the Arndt-Wonacott camera. The wavelength was set to near 1.38 Å. The crystals were maintained at 2°C during data collection. A redundant data set extending to 2.8 Å resolution was obtained from four native crystals covering a total rotation range of 60° about the trigonal c axis, with 1° oscillations for each exposure. A fifth crystal set for rotation about a* covered the blind region and provided scaling data. Heavy atom derivative data were taken on two crystals soaked in

Received May 20, 1988; revision accepted August 3, 1988.

Address reprint requests to Dr. Joël Janin, Laboratoire de Biologie Physicochimique, Université Paris Sud, Centre D'Orsay, 91405 Orsay Cedex, France.

TABLE I. Data Collection

	Resolution (Å)	Reflection number		R merge[a] %	$I > 3\sigma$[b] %
		Total	Independent		
Native	2.8	216,637	63,900	8.5	60
EuCl3	3.0	157,407	52,822	11.0	50
Xylitol	2.2	247,358	120,939	6.4	70

[a]Rmerge = $(\Sigma\ |I_i - \bar{I}|)/(\Sigma I_i)$ is the mean discrepancy between intensity measurements done on equivalent reflections.
[b]Fraction of reflections with intensity larger than 3 times their standard deviations.

10 mM $EuCl_3$, with 50° of c rotation providing most Friedel pairs. Data were also collected on crystals soaked into 0.25 M of the inhibitor xylitol added to the crystallization buffer. Five crystals yielded a set of 0.8° oscillations covering 30° of c rotation, sufficient to provide a complete unique set of data extending to 2.2 Å resolution.

Digitized native and Eu^{3+} films were analyzed and spots were integrated with a version of the OSC program[5,6] given to us by B. Shaanan (Rehovot). On the xylitol films, diffraction spots had to be processed to higher resolution and were more difficult to resolve. These films were analyzed with DENZO, a program kindly given by Z. Otwinowski (Chicago), which included a profile-fitting procedure well suited for densely filled films. Further data processing used the CCP4 software package (CCP4, Daresbury, England). Postrefinement of crystal and beam parameters (Schutt) and the empirical absorption correction of Stuart and Walker[7] were applied to the data. Table I summarizes statistics on integrated intensities.

Phase Determination

Several rare earth ions gave significant, and apparently very similar intensity differences on precession photographs. Eu^{3+} was retained because of its rather large anomalous scattering amplitude at the wavelength chosen. At 2.8 Å resolution, the mean isomorphous difference was 17.6% and the r.m.s. anomalous difference 14% of average F. Isomorphous and anomalous difference Patterson maps were calculated, and one heavy atom site was located in Harker sections. Phases derived from this site led to a difference Fourier map which revealed eight sites in four pairs less than 5 Å apart. These sites were related by noncrystallographic 222 symmetry (n.c.s). Thus, the position and orientation of the molecular two-fold axes of the tetramer were unambiguously defined by the heavy metal sites. The Eu^{3+} positions (Table II) allowed the determination of SIR-AS (single isomorphous replacement - anomalous scattering) phases, which were used to calculate an electron density map to 5 Å resolution (at this resolution the mean figure of merit was 0.52). The map was then averaged about the 222 n.c.s. axes using G. Bricogne's[8] SKEWPLANES procedure. The resulting electron density was very clear; the shape of the protein molecule and its main structural features could easily be identified. The molecular envelope was computed using the reciprocal space version[9] of Wang's[10] automatic procedure. Structure factors ($F\ e^{i\phi c}$) were calculated from the averaged map (truncated by the envelope) and the calculated phases were combined to the SIR-AS phases to recalculate[8,11] a new map with coefficients $(2F_0\text{-}F)\ e^{i\phi}$ comb. The new map was averaged and the procedure was repeated until the figure of merit reached convergence (5 to 6 cycles). The resolution was extended from 5 Å to 2.8 Å in four steps. At each step, 6 cycles of real space averaging were performed starting from SIR-AS phases. At the end of this phase refinement procedure, the mean figure of merit was 0.72 at 2.8 Å resolution.

Model Building and Refinement

The 3 Å electron density map was skeletonized[12] and displayed on the screen of an Evans & Sutherland PS330 graphic system. The polypeptide chain could be traced with little ambiguity, and a polyalanine chain was built by fitting to the skeleton polypeptide chain fragments taken from a data base of protein structures.[13] A detailed model was then built with FRODO[14] by fitting side chains into electron density according to the amino acid sequence of X.I. from *Actinoplanes missouriensis* (to be published elsewhere). Significant electron density was observed for all 394 residues except at the N-terminus, and no deviations from the amino acid sequence were found. As an example Figure 1 shows part of the barrel helix 8 (Table III) fitting nicely in the electron density map. The model was subjected to restrained crystallographic refinement[15] against 2.8 Å native data. Noncrystallographic 222 symmetry was also applied as a restraint. Refinement proceeded smoothly from an initial crystallographic R factor of 37% to a value of 26% at 2.8 Å resolution without manual rebuilding. The model of the native protein described below has a correct stereochemistry, with bond lengths within 0.024 Å r.m.s. from the reference values, bond angles within 2.0° r.m.s. Noncrystallographic symmetry is closely obeyed: equivalent atoms are within 0.04 Å r.m.s. from their mean position after superimposition of the four subunits. Further refinement against xy-

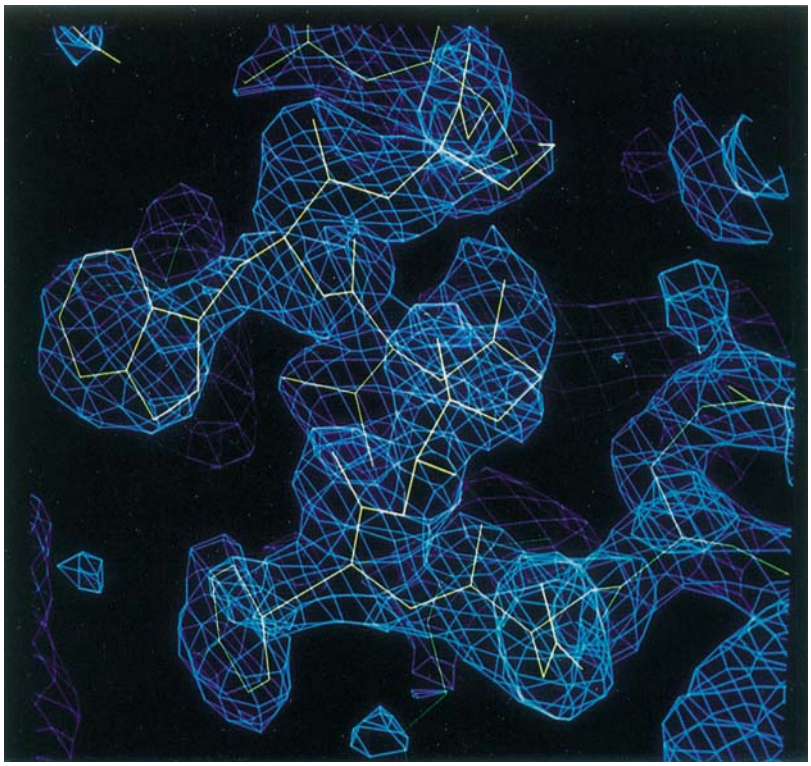

Fig. 1. Fit of helix $\alpha 8$ of the barrel (see Table III) in the 2.8 Å electron density map with n.c.s. refined phases.

TABLE II. Heavy Atom Parameters

Site	X	Y	Z	Occupancy	B (Å^2)
Eu 1	0.455	0.810	0.051	1.8	18
Eu 2	0.476	0.848	0.052	1.8	23
Eu 3	0.403	0.050	0.060	1.6	20
Eu 4	0.388	0.013	0.067	2.0	19
Eu 5	0.618	0.026	0.091	1.7	18
Eu 6	0.586	0.989	0.092	1.8	22
Eu 7	0.346	0.907	0.136	1.9	21
Eu 8	0.321	0.874	0.145	1.6	23

Occupancies are in arbitrary units. Parameters were refined against F_{HLE} coefficients calculated at 3 Å resolution from isomorphous and anomalous differences between native and $EuCl_3$ data. Anomalous data were available for 42% of reflections.

litol data, which extend to higher resolution, is in progress.

Model Analysis

The analysis of the X.I. model was performed using the BRUGEL package[16] and an Evans & Sutherland PS390 graphic system. Molecular graphics tools have been developed within this package (to be published elsewhere) which allow simple geometrical elements such as lines, planes, and cylinders to be superimposed onto user-defined molecular fragments providing valuable assistance in analyzing the molecular organization of complex proteins such as X.I.

RESULTS

Structural Layout

The monomer

A schematic representation of the secondary structure elements in X.I. is given in Figure 2. The X.I. structure comprises two domains: a large N-terminal domain (residues 1–328) forming a parallel eight-stranded α/β barrel and a C-terminal loop (residues 329–394) that extends away from the barrel making extensive contacts with neighboring subunits (Fig. 3).

The boundaries of β strands and α helices forming the barrel are listed in Table III. The Europium ions are bound to carboxylate moieties belonging to residues near the C-terminal ends of β strands $\beta 5$, $\beta 6$, $\beta 7$, and $\beta 8$, thus occupying positions at one side of the β barrel. The binding site for the inhibitor xylitol was identified from a difference Fourier map calculated at 2.8 Å resolution with coefficients from the xylitol and native data and n.c.s. refined phases. Xylitol is an open chain analog of both xylose and xylulose, from which it is derived by reduction of the aldehyde or keto group to an alcohol. The electron density showed that the inhibitor binds next to the metal binding sites at the carboxyl ends of the barrel β strands in

agreement with what is known for other α/β barrel enzymes.[4]

The side of the β sheet surface that packs against the alpha-helices is predominantly hydrophobic. The side that points towards the barrel interior is, on the other hand, highly polar, to allow metal and substrate binding, and thus strongly departs from the average amino acid composition as deduced from analysis of β sheet packing.[17] In agreement with its hydrophilic character a large portion of the barrel interior is exposed to solvent, although water molecules remain excluded from the barrel center, as determined from solvent accessibility calculations.[18] This is an essential requirement in the rationalization of the common geometrical features for a large set of known parallel β barrels.[19]

A comparison of the equatorial cross-sections (sections perpendicular to the barrel axis and passing through the barrel center[19]) in T.I.M. and X.I. shows that they are of similar elliptical shape (Fig. 4) having axial ratios of 1.48 and 1.5, respectively. In the X.I. barrel the area of the equatorial cross-section is 156 Å^2 matching within 4% the average area (163 Å^2) determined in the study referred to above. The average angle of 34° between β strands and the β barrel axis in X.I. is also in agreement with values found for other barrels. However, this angle shows a 13° standard deviation, which is larger than that found for the other β barrels, suggesting that the X.I. barrel is more irregular than for example, the β barrel of T.I.M. Further analysis using a more detailed atomic model will be needed to establish the reason for this observation.

Looking down the barrel in the N- to C-terminal direction, the β strands are ordered in a clockwise fashion, as illustrated in Figure 4. This design principle stems from the right-handed connections between adjacent β strands.[20] Since these connections cannot thread through the closed β sheet surface forming the barrel, the strands must be ordered clockwise.

Despite the similar equatorial shapes of the T.I.M. and X.I. β barrels, the corresponding β strands along the polypeptide chain do not occupy equivalent positions in the barrel. In T.I.M., the first β strand lies

TABLE III. Secondary Structure of X.I.

α/β barrel region (1–328) α helices and β strands	Residues
β1	10– 15
α1	35– 47
β2	49– 54
α2	64– 80
β3	87– 91
α3	108–128
β4	132–138
α4	150–173
β5	177–182
α5	195–206
β6	211–218
α6	227–239
β7	242–247
α7	264–276
β8	288–293
α8	300–328
C-terminal domain (329–394)	

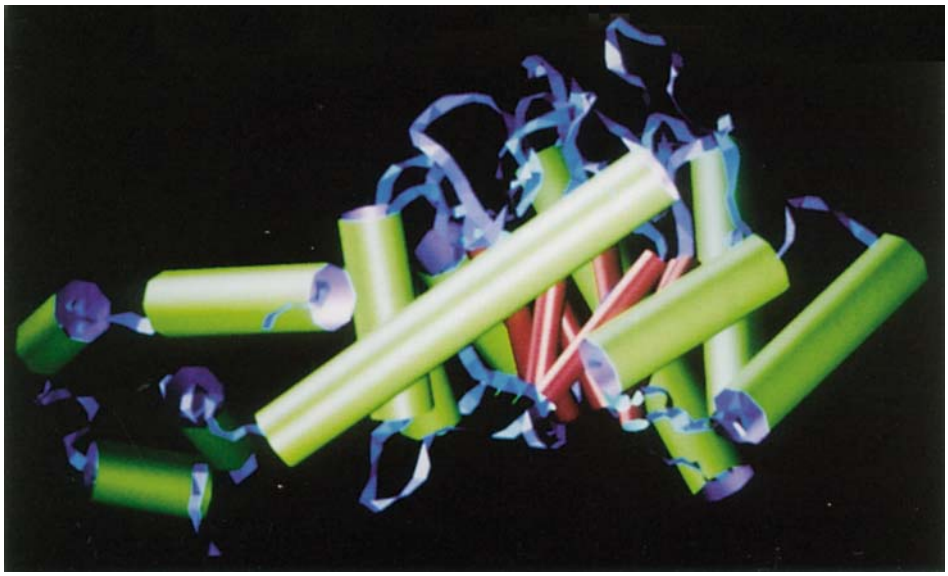

Fig. 2. Ribbon and cylinder representation of the X.I. monomer. The molecule contains an N-terminal eight-stranded α/β barrel domain (center of the picture) followed by a C-terminal loop shaped domain (at the left of the image). The α helices are represented as green hollow cylinders fitted through the Cα atoms, whereas the red cylinders are fitted to the Cα atoms of the β strands. Superimposed on these cylinders is a ribbon representation (in blue) of the main chain. The carboxyl ends of the β strands carrying the active site are pointing upwards.

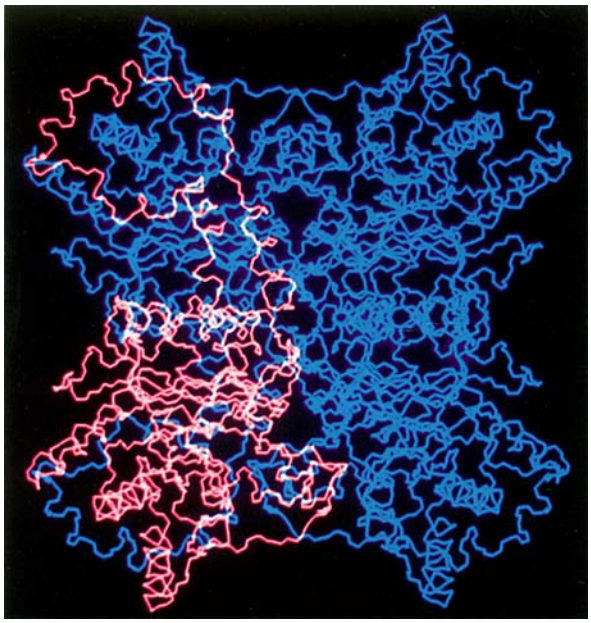

Fig. 3. Backbone tracing of the four subunits of the X.I. tetramer. In order to visualize the organization of the X.I. monomer within the tetrameric structure, one subunit is represented in red while the others are drawn in blue.

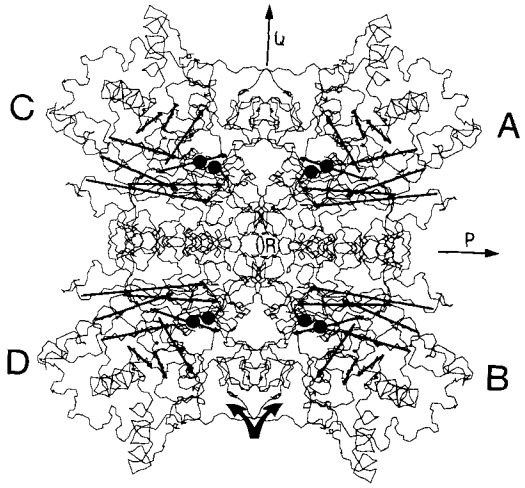

Fig. 5. Backbone tracing of the four subunits (labeled A, B, C, and D) of the X.I. tetramer illustrating the β barrel position in the structure. Least square axes have been drawn through the Cα atoms of the β strands. The arrows on these axes mark the C-terminal ends of the β strands. The double arrow at the bottom of the figure indicates the entrance direction to the active sites of the and B and D subunits. The two-fold symmetry axes P and Q are marked by an arrow. The R axis is perpendicular to the plane of view. Each subunit has two Eu^{3+} binding sites.

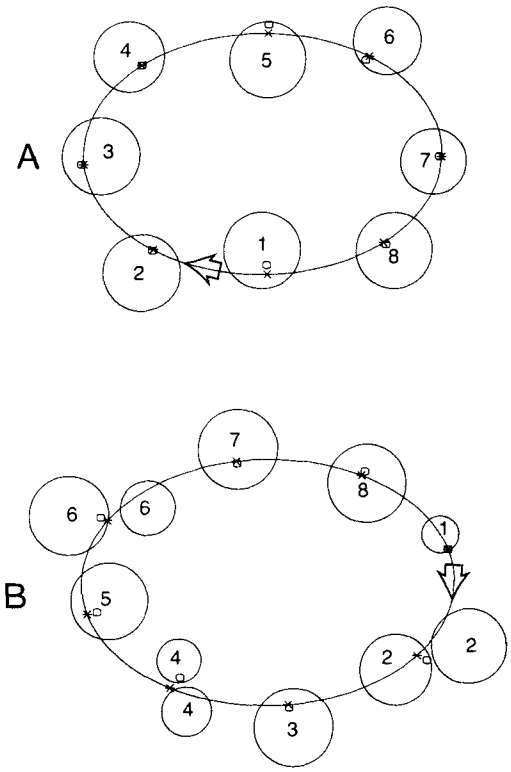

Fig. 4. Cross-sections through β barrels of T.I.M. (a) and X.I. (b). Hyperboloids are fitted to β barrels as described by Lasters et al.[19] Cross-sections shown pass through the equatorial planes of the hyperboloids and are perpendicular to the β barrel axes, with the C-terminii of β strands pointing away from the reader. In these sections the traces of the β strand axes (o) and of the hyperboloid generating lines (x) nearly coincide. Circles represent sections through the Van der Waals spheres of Cα atoms. Both cross-sections are elliptical, but strand 1 lies near the minor axis of the ellipse in T.I.M and near the major axis in X.I.

near the minor axis, whereas in X.I. this strand is located near the major axis (see Figure 4), providing a simple explanation for the finding of Farber et al.[21] that the two protein structures overlap best when the third strand of X.I. is superimposed on the first strand of T.I.M.

Quaternary structure and subunit interactions

The quaternary structure of the X.I. tetramer is characterized by a 222 symmetry relating four identical subunits. The symmetry axes are labeled P, Q, and R on Figure 5, drawn in the PQ plane perpendicular to R. The tetramer has approximately equal dimensions in all directions as can be deduced from the lengths of its semi-axes: a = 44 Å, b = 42 Å, c= 38 Å. Each subunit is involved in extensive contacts with the other three, which cover as much as 39% of its surface. The largest contact occurs between subunits related by symmetry about the P axis, as illustrated in Figure 5. This contact involves the C-terminal loop (residues 329–394), which stretches out of its subunit to cover the surface of its neighbor. In addition, side-by-side contacts occur between helices α4, α5, and α6 of the barrels of both subunits. A quantitative evaluation of the importance of the contact across the P axis is given by its interface area, quoted in Table IV: 4700 Å^2 (per subunit), of which 1650 Å^2 are from residues of the C-terminal loop. This interface area compares with the largest values observed in a survey of oligomeric protein structures by Miller et al.[22] The largest interface occurs in bovine

TABLE IV. Accessible Surface and Subunit Interface Areas

	Surface Area (Å^2)
Accessible surface of:	
Tetramer	48100
Isolated Monomer	19650
Subunit Interface Area:	
P dimer	4700
Q dimer	1600
R dimer	1550
Tetramer	7650

Accessible surfaces are calculated with the Shrake and Rupley[18] algorithm with a probe radius of 1.4 Å. Interface areas are quoted per monomer for each of the three dimers formed by pairs of symmetry related subunits, and for the tetrameric molecule. The P and Q axes are drawn in Figure 5, where the molecule is viewed along the R axis.

catalase and has about the same size as here. The C-terminal loop is also responsible for most of the contacts across the R axis, which is the less extensive of the three. Contacts across the Q axis are different. Pairs of barrels related by the Q axis face each other (Fig. 5) and touch through loops at C-terminal ends of their β strands. The active sites remain nevertheless fully accessible to solvent through a large invagination, the position of which is indicated in Figure 5.

The overall accessible surface area A=48100 Å^2 of the tetramer quoted in Table IV is within 5% of the value expected on the basis of its molecular weight M (173,200) and of an empirical equation:

$$A = 5.3\ M^{0.76} \qquad (1)$$

derived by Miller et al.[22] for oligomeric proteins. X.I. is therefore not different from other oligomers in this respect. In monomeric proteins, a strict correlation also exists between molecular weight and solvent accessible surface area, supporting the idea that the hydrophobicity plays a major part in stabilizing the folded state.[23] In X.I. as in other oligomers,[22] isolated monomers do not obey the correlation. The accessible surface area calculated for a single subunit is 19650 Å^2, 29% more than for a monomeric protein of the same molecular weight. The excess is buried in the subunit contacts, implying that hydrophobicity strongly contributes to subunit association. A hypothetical dimer formed by P related subunits would have an accessible surface area of 29900 Å^2, also close to the value given by Eq.1 for its molecular weight (86600). This suggests that this dimer could form a stable intermediate during tetramer formation thanks to its very large interface and to the C-terminal loops. It is interesting to note that the dimer deviates considerably from sphericity (the semi-axes for the ellipsoid fitting this dimer are a=46 Å, b=35 Å, c=23 Å) supporting the view[22] that the origin of the empirical relation (1) is not simply a consequence of folding a polypeptide chain into a globular structure.

Comparison With Other X.I. Structures

Structural data have been reported for X.I. of *Streptomyces rubiginosus*,[24,25] *Streptomyces olivochromogenes*,[21] and *Arthrobacter*.[25] In the paper on the *Arthrobacter* enzyme, a comparison was made with X.I. from *Streptomyces rubiginosus*. It was concluded that both proteins have a close structural homology. This homology encompasses also the X.I. of *Actinoplanes missouriensis*. The 4 Å resolution Cα coordinates of the *Streptomyces rubiginosus* X.I. (J. Glusker, private communication) were superimposed on our X.I. model. The fit was achieved by the method of least squares on a set of equivalent Cα positions determined by visual inspection in the barrel α helices. When the two models are superimposed, 70% of the 4 Å Cα positions are within less than 1.5 Å of a corresponding Cα in our X.I. model, yielding a total r.m.s. deviation of 0.9 Å. In view of the inherent imperfection of the 4 Å data, this result is very satisfactory. Thus, it may be proposed that the X.I. structures of *Streptomyces rubiginosus*, *Arthrobacter*, and *Actinoplanes missouriensis* are closely related. This assertion can also be extended to X.I. of *Streptomyces olivochromogenes*. The pair of sites binding rare earth ions[26] and the pattern of subunit contacts in the dimer described for this enzyme are in perfect agreement with our findings here.

We note in all published X.I. structures including our own that the second α helix of the barrel is invariably pushed away from the β barrel. This arrangement, probably due to the conformation of the loop preceding this helix, shapes the surface invagination leading to the carboxyl ends of the β barrel. The conservation of this feature further emphasizes the close similarity of presently known X.I. structures.

DISCUSSION

The N-terminal domain of X.I. structure is organized as an eight-stranded α/β barrel, first reported to occur in Triose phosphate isomerase.[3] This folding motif has since then been observed in many other proteins: Pyruvate kinase,[27] KDPG-aldolase,[28] Taka amylase,[29] Glycolate Oxidase,[30] Ribulose-1,5-bisphosphate carboxylase,[31] Flavocytochrome b_2,[32] Muconate lactonizing enzyme,[33] Trimethylamine dehydrogenase,[34] the bifunctional enzyme N-(5′-phosphoribosyl) anthranilate isomerase-indole-3-glycerolphosphate synthase,[35] Tryptophan synthase,[36] Enolase,[37] and muscle Aldolase.[38] Since the amino acid sequences of these proteins display little homology, it has been debated whether these proteins have evolved by convergent evolution.[4]

In a recent study on the structural principles of parallel β barrels,[19] it was suggested that the eight-

stranded barrel geometry can incorporate many different amino acid sequences. The atypical amino acid composition of the X.I. β barrel interior agrees with this view. It is interesting to note that the β strands in the T.I.M. and X.I. barrel are not readily superimposable. From the cross-section plot of Figure 6, it is clear why the best overlap is obtained by matching the first strand of T.I.M. with the third strand of X.I.[21] Interestingly, a similar permutation is needed to superimpose the structures of the Muconate lactonizing enzyme (M.L.E) with T.I.M.[33] M.L.E is a manganese depended enzyme catalyzing the cycloisomerization of cis,cis muconic acid to muconolactone through an enolate intermediate. The fact that the barrels of both X.I. and M.L.E relate in the same manner to the T.I.M. barrel raises the question of whether this structural similarity is due to some common functional features such as metal requirement and/or existence of cyclic reaction intermediates.

From Table III it can be deduced that the regions separating β strands and α helices in X.I. are on the average 13 residues long at the C-terminal sides of the β strands, whereas this average is only 5 residues at the N-terminal sides. In other β barrel proteins, loops at carboxyl ends of β strands are also longer than those at the amino ends. This finding can be correlated with the well-known observation that the active site is positioned invariably at the carboxyl ends of the β barrel strands. These regions may thus account for the specificity of each α/β barrel protein. If the evolution of α/β barrel proteins proceeds through assembly of $\alpha\beta$ building blocks,[39] then it is not surprising that when loop structures are needed to foster *inter* dimer contacts, these are also placed at the C-terminii and *not* at the N-terminii of the β strands. Consequently, the active sites are oriented towards the *inter* dimer contacts, as is shown in Figure 5. It might be speculated that these contacts are needed to spatially constrain the residues in the active site region thereby explaining why X.I. adopts an oligomeric structure in order to function. If this is true, one may question whether the isolated dimer exhibits any enzymatic activity. Nevertheless, our accessible surface calculations suggest that the dimer should be stable. Dissociation of the *Actinoplanes missouriensis* X.I. tetramer requires stringent conditions where the enzymatic activity cannot be measured (unpublished data). Other X.I. enzymes such as that from *E. coli* [40] appear to be dimeric.

Subunit interactions are also important in many other α/β barrel proteins. With the exception of Taka amylase and the bifunctional enzyme mentioned above, all reported α/β barrel proteins are oligomeric. In Triose phosphate isomerase, which is a dimeric protein, a loop of one subunit reaches far into the active site of the other subunit: the conserved[41] Thr at position 75 in this loop forms close interactions with the catalytic residues Lys 13 and His 95 of the other subunit. Possibly the oligomeric nature of most α/β barrel enzymes is due to a stabilization effect of the active site region through subunit contacts. A detailed analysis of the interfaces in all the known oligomeric α/β barrel proteins and structural data on substrate and inhibitor binding will be required to unravel the role played by subunit contacts in enzymatic function.

ACKNOWLEDGMENTS

This work is part of a protein engineering project involving Plant Genetic Systems NV., GIMV (Gewestelijke Investeringsmaatschappij voor Vlaanderen), Gist-Brocades, and Amylum. It has made extensive use of facilities for data collection and processing at LURE, Orsay. We are grateful to its scientific and technical staff for service and help. We also acknowledge the help of the staff of the Laboratoire de Biologie Physicochimique, Orsay, and especially of A. Barneoud, C. Dumas, J. Cherfils, and G. Lebras. Low resolution diffractometer data have been collected at the Institut de Chimie des Substances Naturelles, CNRS, Gif-sur-Yvette, with the competent help of A. Ducruix and B. Arnoux. Film densitometry has been performed at the Centre de Densitometrie, CNRS, Orsay. We thank Drs. G. Bricogne (LURE, Orsay), B. Shaanan (Weizmann Institute, Rehovot), Z. Otwinowski (University of Chicago), A. Leslie (Imperial College, London), and CCP4 (Daresbury, England) for computer programs. Finally, we are grateful to J. Glusker for providing us the 4 Å Cα coordinates of the X.I. from *Streptomyces rubiginosus.*

REFERENCES

1. Kasumi, T.K., Hayashi, K., Tsumura, N. Roles of magnesium and cobalt in the reaction of Glucose isomerase from *Streptomyces griseofuscus* S-41. Agric. Biol. Chem. 46:21–30, 1982.
2. Kasumi, T.K., Hayashi, K., Tsumura, N. Purification and enzymatic properties of Glucose isomerase from *Streptomyces griseofuscus,* S-41. Agric. Biol. Chem. 45:619–627, 1981.
3. Banner, D.W., Bloomer, A.C., Petsko, G.A., Philips, D.C., Pogson, C.I., Wilson, I.A., Corran, P.H., Furth, A.J., Milman, J.D., Offord, R.E., Priddle, J.D., Waley, S.G. Structure of chicken muscle Triose phosphate isomerase determined crystallographically at 2.5 Å resolution using amino acid sequence data. Nature 255:609–614, 1975.
4. Chothia, C. The 14th barrel rolls out. Nature 333:598–599, 1988.
5. Rossmann, M.G. Processing oscillation diffraction data for very large unit cells with an automatic convolution technique and profile fitting. J. Appl. Cryst. 12:225–238, 1979.
6. Schmid, L.H., Weaver, M.A., Holmes, M.G., Gruter, D.H., Ohlendorf, R.A, Reynolds, S.J., Remington, S.J., Mathews, B.W. An oscillation data collection system for high-resolution protein crystallography. Acta Cryst. A37:701–710, 1981.
7. Stuart, D, Walker, N. An empirical method for correcting rotation camera data for absorption and decay effect. Acta Cryst. A35:925–933, 1979.
8. Bricogne, G. Geometric sources of redundancy in intensity data and their use for phase determination. Acta Cryst. A30:395–405, 1974.

9. Leslie, A.G.W. A reciprocal space method for calculating a molecular envelope using the algorithm of B.C. Wang. Acta Cryst. A43:134–136, 1987.
10. Wang, B.C. Resolution of phase ambiguity in macromolecular crystallography. Methods Enzymol. 115:90–112, 1985.
11. Bricogne, G. Methods and programs for direct space exploitation of geometric redundancies. Acta Cryst. A32:832–847, 1976.
12. Greer, J. Computer skeletonization and automatic electron density map analysis. Methods Enzymol. 115:206–224, 1985.
13. Jones, T.A., Thirup, S. Using known substructures in protein model building and crystallography. EMBO J. 5:819–822, 1986.
14. Jones, T.A. Interactive computer graphics:FRODO. Methods Enzymol. 115:157–171, 1985.
15. Hendrickson, W.A., Konnert, J.H. In: "Computing in Crystallography" (Diamond, Ramaseshan and Venkatesan, editors) Indian Academy of Sciences, Bangalore, 1980:13.01–13.25.
16. Delhaise, P., Bardiaux, M., Wodak, S.J. Interactive computer animation of macromolecules. J. Mol. Graph. 2:103–106, 1984.
17. Chothia, C., Janin J. Orthogonal packing of β-pleated sheets in proteins. Biochemistry 21:3955–3965, 1982.
18. Shrake, A., Rupley, J.A. Environment and exposure to solvent of protein atoms. Lysozyme and Insulin. J. Mol. Biol. 79:351–371, 1973.
19. Lasters, I., Wodak, S.J., Alard, P., Van Cutsem, E. Structural principles governing parallel beta barrels in proteins. Proc. Natl. Acad. Sci. USA 85:3338–3342, 1988.
20. Richardson, J.S. The anatomy and taxonomy of protein structure. Adv. Protein Chem. 34:167–339, 1981.
21. Farber, G.K., Petsko, G.A., Ringe, D. The 3.0 Å crystal structure of Xylose isomerase from *Streptomyces olivochromogenes*. Protein Engineering 1:459–466, 1987.
22. Miller, S., Lesk, A.M., Janin, J. The accessible surface area and stability of oligomeric proteins. Nature 328:834–836, 1987.
23. Miller, S., Janin, J., Lesk, A.M., Chothia, C. Interior and surface of monomeric proteins. J. Mol. Biol. 196:641–656, 1987.
24. Carell, H.L., Rubin, B.H., Hurley, T.J., Glusker, J.P. X-ray crystal structure of D-Xylose isomerase at 4 Å resolution. J. Biol. Chem. 5:3230–3236, 1984.
25. Henrick, K., Blow, D.M., Carell, H.L., Glusker, J.P. Comparison of backbone structures of Glucose isomerase from *Streptomyces* and *Arthrobacter*. Protein Engineering 1:467–469, 1987.
26. Farber, G.K., Machin, P., Almo, S.C., Petsko, G.A., Hajdu, J. X-ray Laue diffraction from crystals of Xylose isomerase. Proc. Natl. Acad. Sci. USA 85:112–115, 1988.
27. Stuart, D.I., Levine, M., Muirhead, H., Stammers, D.K. Crystal structure of cat muscle Pyruvate kinase at a resolution of 2.6 Å. J. Mol. Biol. 134:109–142, 1979.
28. Mavridis, I.M., Hatada, M.H., Tulinsky, A., Lebioda, L. Structure of 2-keto-3-deoxy-6-phosphogluconate Aldolase at 2.8 Å resolution. J. Mol. Biol. 162:419–444, 1982.
29. Matsuura, Y., Kusunoki, L., Harada., W., Tanaka, N., Iga, Y., Yanaka, N., Toda, H., Narita, K., Kakudo, M.J. Molecular structure of Taka-amylase A. Biochem (Tokyo) 87:1555–1558, 1980.
30. Lindqvist, Y., Branden, C.I. Structure of Glycolate oxidase from spinach. Proc. Natl. Acad. Sci. USA 82:6855–6859, 1985.
31. Schneider, G., Lindqvist, Y., Branden, C.I., Lorimer, G. Three-dimensional structure of Ribulose-1,5-bisphosphate carboxylase/oxygenase from Rhodospirillum rubrum at 2.9 Å resolution. EMBO J. 5:3409–3415, 1986.
32. Xia, Z.X., Shamala, N., Bethge, P.H., Lim, L.W., Bellamy, H.D., Xuong, N.H., Lederer, F., Mathews, F.S. Three-dimensional structure of Flavocytochrome b_2 from baker's yeast at 3.0 Å resolution. Proc. Natl. Acad. Sci. USA 84:2629–2633, 1987.
33. Goldman, A., Ollis, D.L., Steitz, T.A. Crystal structure of Muconate lactonizing enzyme at 3 Å resolution. J. Mol. Biol. 194:143–153, 1987.
34. Lim, L.W., Shamala, N., Mathews, F.S., Steenkamp, D.J., Hamlin, R., Xuong, N.H. Three-dimensional structure of the iron-sulfur Flavoprotein trimethylamine dehydrogenase at 2.4 Å resolution. J. Biol. Chem. 261:15140–15146, 1986.
35. Priestle, J.P., Grutter, M.G., White, J.L., Vincent, M.G., Knia, M., Wilson, E., Jardetzky, T.S., Kirschner, K., Jansonius, J.N. Three-dimensional structure of the bifunctional enzyme N-(5'-phosphoribosyl) anthranilate isomerase-indole-3-glycerol-phosphate synthase from Escherichia coli. Proc. Natl. Acad. Sci. USA 84:5690–5694, 1987.
36. Hyde, C.C., Padlan, E.A., Ahmed, S.A., Miles, E.W., Davies, D.R. Three-dimensional structure of the tryptophan synthase α_2–β_2 complex from Salmonella at 2.8 Å resolution. Fedn. Proc. 46:2215, 1987.
37. Lebioda, L., Stec, B. Crystal structure of Enolase indicates that Enolase and Pyruvate kinase evolved from a common ancestor. Nature 333:683–685, 1988.
38. Sygusch, J., Beaudry, D., Allaire, M. Molecular architecture of rabbit skeletal muscle Aldolase at 2.7 Å resolution. Proc. Natl. Acad. Sci. USA 84:7846–7850, 1987.
39. Lornberg, N., Gilbert, W. Intron/exon structure of the chicken Pyruvate kinase gene. Cell 40:81–90, 1985.
40. Tucker, M.Y., Tucker, M.P., Himmel, M.E., Grohmann, K., Lastick, S.M. Properties of genetically overproduced E. Coli Xylose isomerase. Biotechnol. Lett. 10:79–84, 1988.
41. Swinkels, B.W., Gibson, W.C., Osinga, K.A., Kramer, R., Veeneman, G.H., Van Boom, J.H., Borst, P. Characterization of the gene for the microbody (glycosomal) Triose phosphate isomerase of Trypanosoma brucei. EMBO J. 5:1291–1298, 1986.